



**HAL**  
open science

# Study of Atmospheric Turbidity in a Northern Tropical Region Using Models and Measurements of Global Solar Radiation

Mohamed Zaiani, Abdanour Irbah, Djelloul Djafer, Constantino Listowski,  
Julien Delanoë, Dimitris Kaskaoutis, Sabrina Belaid Boualit, Fatima  
Chouireb, Mohamed Mimouni

## ► To cite this version:

Mohamed Zaiani, Abdanour Irbah, Djelloul Djafer, Constantino Listowski, Julien Delanoë, et al.. Study of Atmospheric Turbidity in a Northern Tropical Region Using Models and Measurements of Global Solar Radiation. *Remote Sensing*, 2021, 13, pp.2271. 10.3390/rs13122271 . insu-03258792

**HAL Id: insu-03258792**

**<https://insu.hal.science/insu-03258792>**

Submitted on 11 Jun 2021

**HAL** is a multi-disciplinary open access archive for the deposit and dissemination of scientific research documents, whether they are published or not. The documents may come from teaching and research institutions in France or abroad, or from public or private research centers.

L'archive ouverte pluridisciplinaire **HAL**, est destinée au dépôt et à la diffusion de documents scientifiques de niveau recherche, publiés ou non, émanant des établissements d'enseignement et de recherche français ou étrangers, des laboratoires publics ou privés.



Distributed under a Creative Commons Attribution - NoDerivatives 4.0 International License



## Article

# Study of Atmospheric Turbidity in a Northern Tropical Region Using Models and Measurements of Global Solar Radiation

Mohamed Zaiani <sup>1,\*</sup>, Abdanour Irbah <sup>2</sup>, Djelloul Djafer <sup>1</sup>, Constantino Listowski <sup>2</sup>, Julien Delanoe <sup>2</sup>, Dimitris Kaskaoutis <sup>3,4</sup>, Sabrina Belaid Boualit <sup>1</sup>, Fatima Chouireb <sup>5</sup> and Mohamed Mimouni <sup>6</sup>

- <sup>1</sup> Unité de Recherche Appliquée en Energies Renouvelables, URAER, Centre de Développement des Energies Renouvelables, CDER, Ghardaïa 47133, Algeria; adjafer@yahoo.com (D.D.); sabriboualit@gmail.com (S.B.B.)
- <sup>2</sup> LATMOS/IPSL, UVSQ Université Paris-Saclay, Sorbonne Université, CNRS, 11 BD D'Alembert, 78280 Guyancourt, France; Abdenour.Irbah@latmos.ipsl.fr (A.I.); constantino.listowski@latmos.ipsl.fr (C.L.); Julien.Delanoe@latmos.ipsl.fr (J.D.)
- <sup>3</sup> Institute for Environmental Research and Sustainable Development, National Observatory of Athens, Palaia Penteli, 15236 Athens, Greece; dkask@noa.gr
- <sup>4</sup> Environmental Chemical Processes Laboratory, Department of Chemistry, University of Crete, 71003 Crete, Greece
- <sup>5</sup> Laboratoire des Télécommunications, Signaux et Systèmes LTSS, Université Amar Telidji, Laghouat 03000, Algeria; f.chouireb@lagh-univ.dz
- <sup>6</sup> Office National de la Météorologie, Direction Régionale Sud, Tamanrasset 11000, Algeria; m\_mimouni\_dz@yahoo.fr
- \* Correspondence: zaianimo@gmail.com



**Citation:** Zaiani, M.; Irbah, A.; Djafer, D.; Listowski, C.; Delanoe, J.; Kaskaoutis, D.; Boualit, S.B.; Chouireb, F.; Mimouni, M. Study of Atmospheric Turbidity in a Northern Tropical Region Using Models and Measurements of Global Solar Radiation. *Remote Sens.* **2021**, *13*, 2271. <https://doi.org/10.3390/rs13122271>

Academic Editor: Didier Gillotay

Received: 2 May 2021

Accepted: 6 June 2021

Published: 10 June 2021

**Publisher's Note:** MDPI stays neutral with regard to jurisdictional claims in published maps and institutional affiliations.

**Copyright:** © 2021 by the authors. Licensee MDPI, Basel, Switzerland. This article is an open access article distributed under the terms and conditions of the Creative Commons Attribution (CC BY) license (<https://creativecommons.org/licenses/by/4.0/>).

**Abstract:** Radiative transfer in the Earth's atmosphere under clear-sky conditions strongly depends on turbidity due to aerosols and hydrometeors. It is therefore important to know its temporal radiative properties for a given site when the objective is to optimize the solar energy that is collected there. Turbidity can be studied via measurements and models of the global solar radiation reaching the ground in cloudless conditions. These models generally depend on two parameters, namely the Angström turbidity coefficient and the Linke factor. This article aims to do a comparative study of five models of global solar radiation, all dependent on the Linke factor, based on real data. The measurements are provided by the Tamanrasset Meteorological Center (Algeria), which has a long series of global solar radiation data recorded between 2005 and 2011. Additional data from AERONET and MODIS onboard the TERRA satellite were also used to perform the comparison between the two estimated parameters and those obtained from AERONET. The study shows that the ESRA models are the most reliable among the five models for estimating the Linke factor with a correlation coefficient  $R$  of the data fits of 0.9995, a RMSE of 13.44 W/m<sup>2</sup>, a MBE of −0.64 W/m<sup>2</sup> and a MAPE of 6.44%. The maximum and minimum statistical values were reached, respectively, in June and during the autumn months. The best correlation is also observed in the case of ESRA models between the Linke parameter and the joint optical thickness of aerosols and the total column-integrated water vapor. The Angström turbidity coefficient  $\beta$ , calculated from the Linke factor and MODIS data, has values less than 0.02 at 9% of the cases, and 76% present values ranging between 0.02 and 0.15 and 13% higher than 0.15. These  $\beta$  values are validated by AERONET measurements since a very good correlation ( $R \approx 0.87$ ) is observed between the two datasets. The temporal variations of  $\beta$  also show a maximum in June. Satellite observations confirm more aerosols during the summer season, which are mostly related to the African monsoon.

**Keywords:** linke turbidity; angstrom coefficient; clear sky model

## 1. Introduction

Atmospheric transparency can be affected both by natural phenomena within the Earth's atmosphere (clouds, dust, etc.) and by human activity (factories, cars, etc.). These effects and their variations over time must be taken into account in climate models or

pollution studies [1], as well as when receiving or transmitting beams through the atmosphere from the Earth to space and vice versa. This is particularly the case when installing solar energy conversion systems where the efficiency of the solar collectors is affected by atmospheric turbidity and weather conditions [2,3]. Indeed, solar irradiance at ground level is highly dependent on the Earth's atmospheric turbidity [4]. The quality and amount of solar radiation passing through the atmosphere is altered by atoms and molecules (ozone, water vapor, carbon dioxide . . .) that are present along the propagation path but also by liquid and solid aerosols that can be either dispersed or grouped in clouds. Hydrometeors and aerosols are responsible for the turbidity of the atmosphere that makes it more or less opaque to radiation [5–8]. It is therefore important to quantify their effects when recording solar irradiance in a given location. Several broadband models were developed to predict solar irradiance at the Earth's surface under cloudless conditions [9–13]. They mainly depend on parameters related to the turbidity. Different parameters based on radiometric methods have been defined to evaluate the atmospheric turbidity linked to the attenuation of solar radiation reaching the Earth's surface due to hydrometeors and aerosols in the atmosphere [14]. The most common parameters used are the Linke turbidity factor,  $T_l$  [15], and the Angström turbidity coefficient,  $\beta$  [16]. The Linke turbidity factor describes the optical thickness of the atmosphere due to both absorption by water vapor and absorption/scattering by aerosols suspended in the atmosphere [17]. The Angström turbidity coefficient is a parameter that characterizes the aerosol content in a given vertical column of air in the atmosphere and practically refers to the attenuation of solar light at 1 micrometer [1]. These turbidity indices have been widely used at several places around the world based on solar irradiance measurements in order to quantify the effects of aerosols and air pollutants on degrading horizontal visibility and reducing the amount of solar radiation reaching the ground. In this respect, variations in the Linke turbidity factor have been studied by Cucumo et al. [18] at two locations in Italy, while Djafer and Irbah [19], Marif et al. [20], Chabane et al. [21] analyzed the characteristics and seasonality of the Linke turbidity factor at several sites in Algeria. In Tunisia, Saad et al. [22] quantified the atmospheric turbidity by means of both the Linke turbidity factor and the Angstrom coefficient, while Kambezidis and Psiloglou [23] in a recent study estimated and mapped the Linke turbidity factor at 33 sites across Greece. Several other studies have dealt with analysis of the Linke turbidity factor at several places around the world like in Egypt [24], in Chile [25], and in Brazil [26].

This article deals with the estimation of the Linke turbidity factor and the Angström coefficient considering both models and measurements of global solar radiation reaching the ground under clear-sky conditions. Five models are therefore considered and compared to obtain the best estimates of the Linke turbidity factor and hence the Angström coefficient. We first describe the turbidity models used in this work and present the results obtained following the analysis of solar radiation measurements recorded over the period 2005–2011 from a radiometric station located in Tamanrasset, southern Algeria. The results are then discussed and compared with both AERONET (AEROSOL ROBOTIC NETWORK) measurements obtained on the same site and with data recorded from space.

## 2. Turbidity Models

The Linke turbidity factor is obtained by fitting measurements of global solar radiation through methods of least squares using one of five models as described below.

### 2.1. The Gistel Model

The Gistel clear sky model is the model adopted by the World Organization of Meteorology (WMO) [27]. The global solar radiation  $G_c$ , which in this model depends mainly on the Linke turbidity factor  $T_l$ , is expressed by the equation:

$$G_c = \epsilon(1300 - 75T_l)(\sin(h))^{(36+T_l)/33} \quad (1)$$

where  $h$  is the Sun's elevation angle and  $\epsilon$  is the correction factor for the Earth–Sun distance given by:

$$\epsilon = 1 + 0,034\cos(-0.986(d - 3)) \quad (2)$$

where  $d$  is the number of days in a year.

### 2.2. The Kasten Model

This model also depends mainly on the Linke turbidity factor  $T_l$ . The global solar radiation  $G_c$  is expressed by [28,29]:

$$G_c = I_0 \sin(h) 0.84 \exp[-0.027 T_l / \sin(h)] \quad (3)$$

where  $I_0$  is the Total Solar Irradiance (TSI) equal to 1361 W/m<sup>2</sup> and  $h$  is the Sun's elevation angle.

### 2.3. The ESRA 1 Model

In this model, the global solar irradiance  $G_c$  for clear sky is split into two parts: the direct component,  $B_c$ , and the diffuse component,  $D_c$ , which are determined separately:

$$G_c = B_c + D_c$$

The direct irradiance on a horizontal surface (or beam horizontal irradiance) for clear sky is given by [30]:

$$B_c = I_0 \epsilon \sin(h) \exp(-0.8662 T_l m \delta) \quad (4)$$

where  $I_0$ ,  $\epsilon$ , and  $\delta$  are the Total Solar Irradiance (TSI), the correction factor Earth-Sun distance, and the integral of the Rayleigh optical thickness, respectively.  $h$  is the Sun's elevation angle and  $m$  is the optical air mass given by :

$$m = m_r \frac{P}{101325} \quad (5)$$

$m_r$  and  $P$  are the relative air mass and pressure, given, respectively, by:

$$m_r = \frac{1}{\sin(h) + 0.50572(h + 6.07995)^{-1.6364}} \quad (6)$$

$$P = 101325 \exp(-0.0001184 alt) \quad (7)$$

where  $alt$  is the altitude of the area.

The diffuse horizontal irradiance  $D_c$  is determined by:

$$D_c = I_0 \epsilon T_{rd}(T_l) F_d \quad (8)$$

where  $T_l$  is the Linke turbidity factor.

The diffuse radiation is expressed in Equation (8) as the product of the diffuse transmission function at zenith  $T_{rd}$  by a diffuse angular function  $F_d$ :

$$T_{rd}(T_l) = -1.5843 \times 10^{-2} + 3.0543 \times 10^{-2} T_l + 3.797 \times 10^{-4} T_l^2 \quad (9)$$

$$F_d = A_0 + A_1 \sin(h) + A_2 (\sin(h))^2 \quad (10)$$

where  $h$  is the Sun's elevation angle. The coefficients  $A_0$ ,  $A_1$ , and  $A_2$  depend solely on the Linke turbidity factor  $T_l$ . They are unitless and are given in [30].

#### 2.4. The ESRA 2 Model

The ESRA 2 model is very similar to ESRA 1 but with a variant to calculate  $B_c$  using the following equations [30]:

$$B_c = I_0 \epsilon T_{rb}(T_l) F_b(h, T_l) \quad (11)$$

where  $h$ ,  $I_0$ , and  $\epsilon$  are the Sun's elevation angle, the TSI, and the correction factor for Earth–Sun distance, respectively.  $T_{rb}$  is a transmission function for beam radiation at zenith, and  $F_b$  is a beam angular function, given by :

$$T_{rb}(T_l) = \exp[-0.8662T_l(p/p_0)\delta] \quad (12)$$

$$F_b(h, T_l) = C_0 + C_1 \sin(h) + C_2 (\sin(h))^2 \quad (13)$$

The coefficients  $C_0$ ,  $C_1$ , and  $C_2$ , which depend on the Linke turbidity factor  $T_l$  and air mass, were computed for three ranges of the Sun's elevation angle: at noon below  $15^\circ$ , between  $15^\circ$  and  $30^\circ$  and over  $30^\circ$ . These coefficients are given in [30].

#### 2.5. The Capderou Model

Capderou proposed a parametric model based on the Linke turbidity factor  $T_l$  [31]. This model is essentially produced for Algeria in the Algerian solar atlas [31–33]. The Linke turbidity used by the model is a combination of atmospheric turbidity due to water vapor absorption, molecular diffusion, and aerosol diffusion associated with some slight absorption [32,33]. This model is based on the theoretical approach of Perrin de Brichambaut and Vauge [34]. The expression for direct solar radiation under cloudless sky conditions  $B_c$  is given by:

$$B_c = I_0 \epsilon \cos(\theta) \exp[-T_l m \delta] \quad (14)$$

where  $I_0$ ,  $\epsilon$ ,  $\theta$ ,  $m$  and  $\delta$  are the TSI, the correction factor Earth-Sun distance, the incidence angle (in degrees), the optical air mass and the integral of the Rayleigh optical thickness, respectively.

The diffuse solar radiation on a horizontal plane  $D_c$  is given by the following equation:

$$D_c = I_0 \exp(-1 + 1.06 \log(\sin(h))) + a - \sqrt{a^2 + b^2} \quad (15)$$

where  $a$  and  $b$  are coefficients obtained from [32,33].  $h$  is the Sun's elevation angle.

The global horizontal solar radiation  $G_c$  is then obtained by:

$$G_c = B_c + D_c$$

### 3. Used Data and Site Location

The models described in the previous section are used to fit the global solar irradiance measurements with methods of least squares in order to estimate the Linke turbidity factor. The data needed for this work are first presented.

#### 3.1. Aeronet and Modis Data

Photometer measurements of the direct (collimated) solar radiation from the AERONET network (<http://aeronet.gsfc.nasa.gov>, accessed on 1 March 2021) provide information to calculate the columnar Aerosol Optical Depth (AOD) at different wavelengths ( $\lambda$ ). AOD and  $\lambda$  are used to compute the Angström turbidity ( $\alpha$  exponent,  $\beta$  coefficient) thanks to the Angström relationship (Equation (16)). Two data versions (1 and 2) and three levels (1.0, 1.5, 2.0) exist for each product. The highest quality data can be found in version 2, level 2.0, following a delay of 12 months or longer (due to final calibration and manual inspection). This product is used in this work for the Tamanrasset region (see Figure 1)

to obtain the AOD at 870 nm, for which there are 571 measurements over the period 01/01/2007–31/12/2011, except for 2010, for which no measurements are available.

$$AOD = \beta\lambda^{-\alpha} \quad (16)$$

The present study also makes use of 10 km-resolution level 2.0 products MOD07 of total column-integrated water vapor  $W_v$  acquired between 2005 and 2011 obtained from MODIS sensor on the TERRA spacecraft [35].

Figure 2 plots the monthly average of AOD obtained from AERONET on the left-hand side, and the average of the total column-integrated water vapor  $W_v$  obtained from MODIS on the right-hand side, over the period of 2005–2011.



Figure 1. Site location.

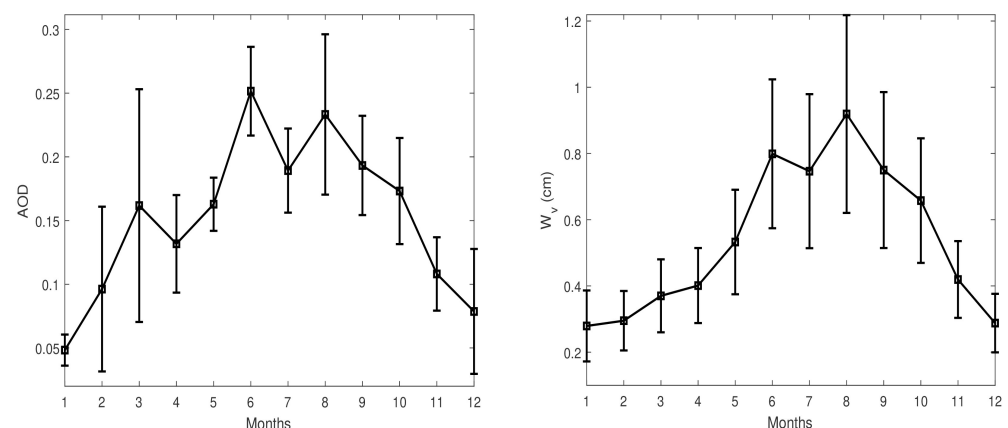


Figure 2. Monthly average of AERONET AOD (left) and of MODIS water vapor (right).

### 3.2. Ground-Based Solar Radiation Data

Solar data were collected between 01/01/2005 and 31/12/2011 at Tamanrasset (22.79°N, 5.53°E, 1377 m a.s.l., Figure 1) in southern Algeria very close to the Tropic of Cancer, by the Regional Meteorological Center (Direction météo Régional Sud, Office National de la Météorologie, ONM, Algeria). The data correspond to measurements of direct, global and

diffuse solar radiation. Instruments and methods for data collection are the same as those described in detail in Zaiani et al. [36]. The main difference is that the three components of solar radiation are recorded every minute at Tamanrasset together with temperature, humidity and pressure. Instruments that measure direct, global and diffuse solar radiation components are EKO-type instruments (<http://eko-eu.com/>, accessed on 1 March 2021). They are calibrated every three years and cleaned two to three times a week depending on weather conditions. The whole dataset used in this work consists of 2191 days of global solar radiation measurements. However, only clear days are considered to study the turbidity. They are selected from the dataset according to an appropriate method [37], thereby reducing the number of useful days to 870, that is to say, that 40% of the observed days at Tamanrasset are determined to be clear.

#### 4. Results and Discussion

The dataset of global solar radiation measurements described in the previous section was processed using the five models (see Section 2) to estimate the Linke turbidity factor  $T_l$  for Tamanrasset. A first analysis of the results reported in Table 1 was then carried out using several metric parameters, which are the *root mean square error (RMSE)*, the *mean absolute percentage error (MAPE)*, the *dependence of model error (MBE)* and the *correlation coefficient (R)* (see Zaiani et al. [36] for definitions). With regard to these parameters, it can be seen that the ESRA 2 model fits better overall to global measurements of solar radiation than the other models. Indeed, in this case we have  $RMSE \approx 13.44 \text{ W/m}^2$ ,  $MAPE \approx 6.44\%$ ,  $MBE \approx -0.64 \text{ W/m}^2$  and a mean  $R$  of 0.9995. On the other hand, Kasten's model is the one that has the relatively worst values for  $RMSE$  and  $R$ .

**Table 1.** Average errors in the estimation of the Linke turbidity.

Errors/Models	Kasten	Gistel	ESRA1	ESRA2	Capderou
$RMSE \text{ (W/m}^2\text{)}$	29.52	18.34	14.84	13.44	16.13
$MAPE \text{ (}\%\text{)}$	10.34	10.95	12.50	6.44	15.22
$MBE \text{ (W/m}^2\text{)}$	1.03	4.26	2.58	-0.64	3.82
$R$	0.9981	0.9991	0.9994	0.9995	0.9993

The statistical analysis was then continued by calculating both its monthly average over time and the histogram of its values. A comparative study between the Linke turbidity and two closely related parameters ( $AOD$ ,  $W_v$ ) was conducted afterwards to differentiate the models.

Figure 3 plots the monthly average values of the Linke turbidity factor calculated over the period 2005–2011 with the five models. We can notice that they have a similar annual variability with mean values, however different, but the Capderou model seems to behave differently from the others. We observe that the Linke turbidity factor peaks in June, while it decreases during the winter months. A local maximum seems to occur in September–October, although it is not clearly apparent for all models. The results also show that the Linke turbidity factor obtained from the models has clearly visible differences in its histograms of values (top plots in Figure 4). This is best seen in the bottom plot in Figure 4, where the kernel densities of all models are plotted in the same frame. We observe a clear bias in the values of the Linke turbidity factor obtained with the model of Kasten, but also with that of Gistel, albeit smaller, as confirmed by the occurrences of  $T_l$  values. Of the  $T_l$  values, 55.50%, 18.92%, 5.38%, 6.88% and 4.47% are less than 2 for models Kasten, Gistel, ESRA1, ESRA2 and Capderou respectively; 39.67%, 76.03%, 71.33%, 70.18% and 75% are between 2 and 4; and 1.49%, 4.71%, 21.33%, 20.98%, 19.26% greater than 4.

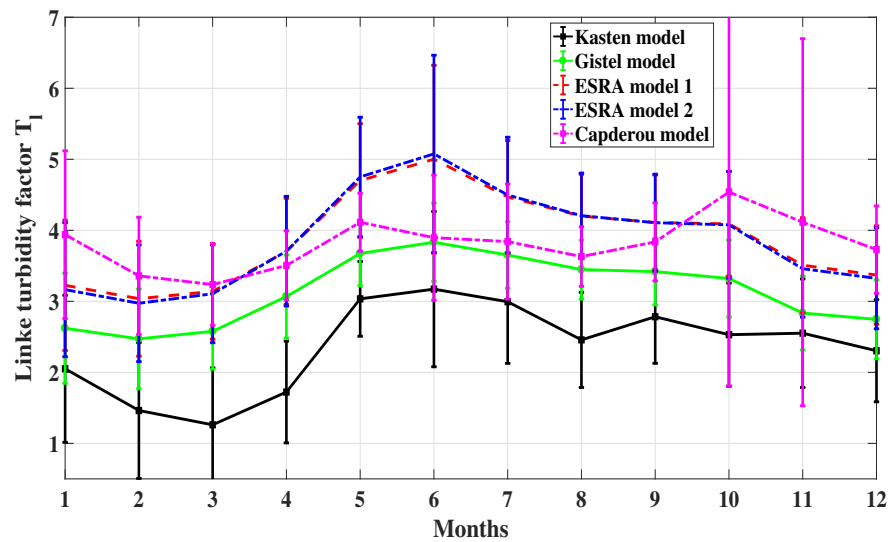


Figure 3. Monthly average of the Linke turbidity factor.

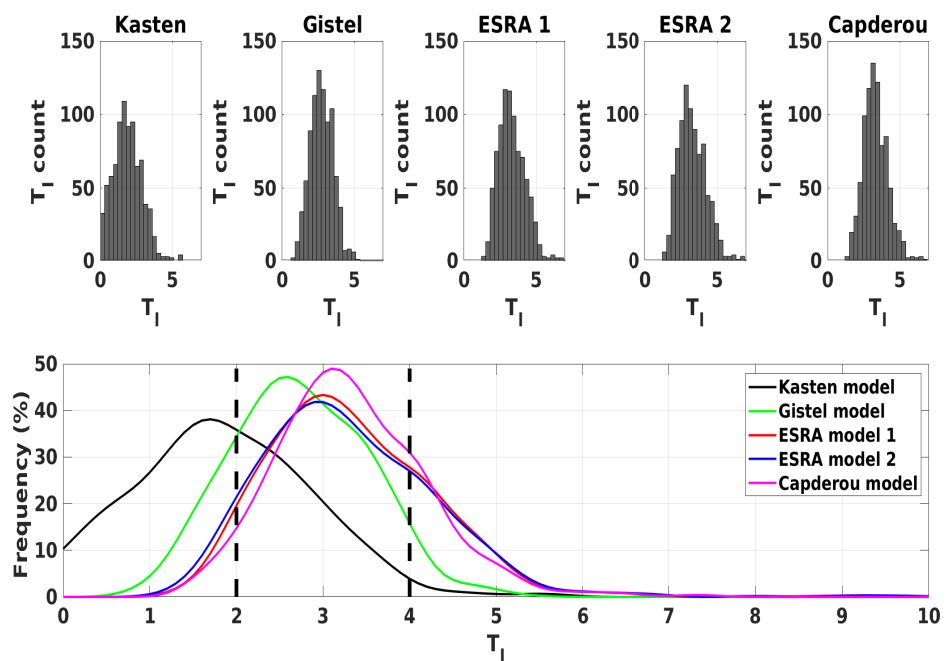


Figure 4. Histograms of Linke turbidity factor obtained with each model for the period 2005–2011.

The disparity in results shows the need to find the most reliable model for estimating the Linke turbidity factor from global solar radiation measurements. The ESRA 1 and ESRA 2 models give similar results, and from here on only the ESRA 2 model will be considered. The optical depth of aerosols and the total column-integrated water vapor will be used to find the most relevant model for Tamanrasset. On clear days, these parameters have a significant effect on the propagation of solar radiation in the atmosphere (see Section 1) and therefore strongly affect the Linke turbidity factor. To perform this comparison, the joint transmittance  $\tau_{wa}$  of both the water vapor and aerosol particles is calculated as follows:

$$\tau_{wa} = \tau_w \tau_a \quad (17)$$

where  $\tau_w$  and  $\tau_a$  are the transmittances of water vapor and aerosols, respectively.

- $\tau_w$  is obtained using the formula given in Iqbal [38] of the transmittance following absorption by water vapor:

$$\tau_w = 1 - 2.4959U_w[(1 + 79.03U_w)^{0.6828} + 6.385U_w]^{-1} \quad (18)$$

where  $U_w$  is the pressure-corrected relative optical path length for water vapor:

$$U_w = W_v m \quad (19)$$

where  $W_v$  is the total column-integrated water vapor abundance and  $m$  the optical air mass.

- $\tau_a$  is calculated through the transmittance formula given in Louche [39] of aerosol scattering and is dependent on the optical air mass  $m$ , the Angström coefficient  $\beta$  and the Angström exponent  $\alpha$ :

$$\tau_a = (0.12445\alpha - 0.0162) + (1.003 - 0.125\alpha)\exp[-\beta m(1.089\alpha + 0.5123)] \quad (20)$$

$\tau_a$  and  $\tau_w$  are calculated using  $(\beta, \alpha)$  from AERONET and using the total column-integrated water vapor given by MODIS ( $w = W_v$ ). Indeed, the last parameter calculated with meteorological data recorded at Tamanrasset using Equation (9) of Djafer and Irbah [19] is very close to that of MODIS (Figure 5).

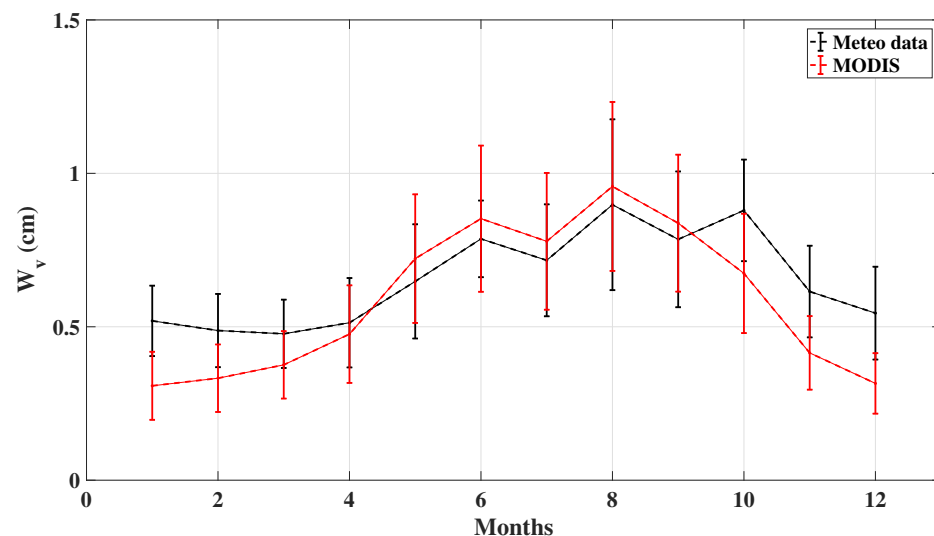


**Figure 5.** Monthly values of the total column-integrated water vapor obtained from the meteorological data recorded at Tamanrasset and from MODIS.

The Linke turbidity factor  $T_l$  can therefore be compared with  $\log(\tau_{wa})$  given that the transmittance  $\tau_{wa}$  is related to the exponential of the Optical Thickness of Atmospheric Components (OTAC):

$$\tau_{wa} = e^{-(OTAC)} \quad (21)$$

where  $OTAC$  refers here to water vapor and aerosols.

Note that this comparison is performed to reveal the similarity in the variation between  $T_l$  and  $\log(\tau_{wa})$ , where the same trend is expected. The left plots in Figure 6 show both the monthly average values of the Linke turbidity factor and  $\log(\tau_{wa})$  for each model. The Gistel and ESRA models appear to have a better agreement between  $T_l$  and  $\log(\tau_{wa})$  compared to the Kasten and Capderou models. Indeed, they have very similar results and give the monthly mean value with the highest Linke turbidity factor of the year (June), which coincides with the highest  $\log(\tau_{wa})$  value. The middle plots in Figure 6

show the linear regression performed on monthly average values of the Linke turbidity factor and  $\log(\tau_{wa})$ . The results confirm the good correlation between  $T_l$  and  $\log(\tau_{wa})$  in the case of the Gistel and ESRA models compared to the others. Indeed, the Gistel and ESRA models have correlation coefficients  $R$  of 0.91 and 0.93, respectively. These results are confirmed by plotting the linear regression performed on the daily data of the Linke turbidity factor and the  $\log(\tau_{wa})$  (see the right plots of Figure 6). The  $R$  values are then 0.56 and 0.61, respectively, for the Gistel and ESRA models. We also note, as expected, that the Linke turbidity factor determined with the Capderou model has the worst correlation with  $\log(\tau_{wa})$ , where  $R$  is 0.25 and 0.15 when the monthly and daily mean values are taken, respectively. We conclude that the Gistel and ESRA models are more suitable for the estimation of the Linke turbidity factor than the others studied in this work, with the ESRA model performing the best. The ESRA model is therefore considered from here on.

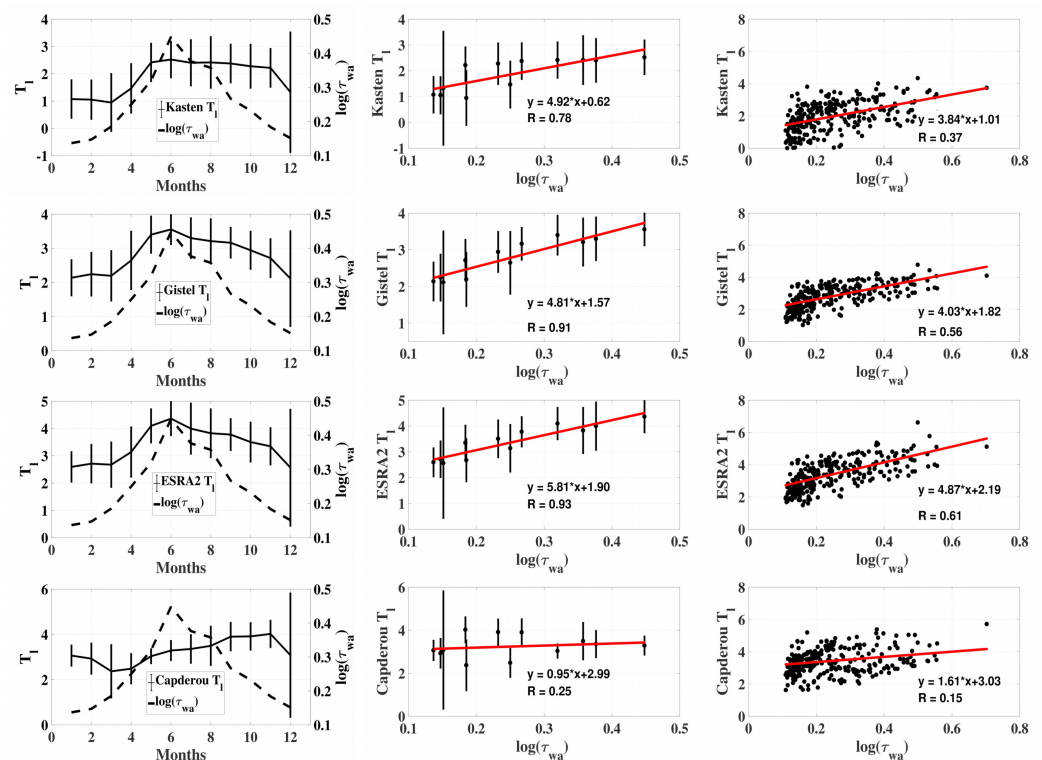


**Figure 6.** Left plots: monthly average values of both the Linke turbidity (full line) and  $\log(\tau_{wa})$  (dashed line). Middle plots: correlation between the monthly average values of the Linke turbidity and  $\log(\tau_{wa})$ . Right plots: correlation between the daily values of the Linke turbidity and  $\log(\tau_{wa})$ .

The  $T_l$  value obtained with the ESRA model makes it possible to deduce the Angström turbidity coefficient  $\beta$  that characterizes the amount of aerosol in the atmosphere in the column direction.  $\beta$  is calculated according to the following empirical formula [40]:

$$\beta = \frac{T_l - \left[ \frac{h+85}{39.5 \exp(-w_p) + 47.4} + 0.1 \right]}{16 + 0.22w_p} \quad (22)$$

where  $h$  is the Sun elevation angle in degrees and  $w_p$  the precipitation amount in centimeters.  $w_p$  values are also taken from MODIS ( $w_p = W_v$ ).

The left plot in Figure 7 shows the daily variation in the Angström coefficient calculated for Tamanrasset during the period 2005–2011 using Equation (22). We note that values range from 0.03 to 0.25 with a mean value of 0.08. The histogram of daily  $\beta$  values is shown in the right plot. It reveals that 9% of Angström coefficient values at Tamanrasset are less than 0.02, 76% are between 0.02 and 0.15, and 13% are higher than 0.15. We can compare

these results with those of Ghardaïa, located about 1100 km northward Tamanrasset. Djafer and Irbah [19] found that 9.4% of Angström turbidity coefficient values are less than 0.02, 75.4% are between 0.02 and 0.15 and 15.2% exceed 0.15. We observe that the results from both regions are very close.

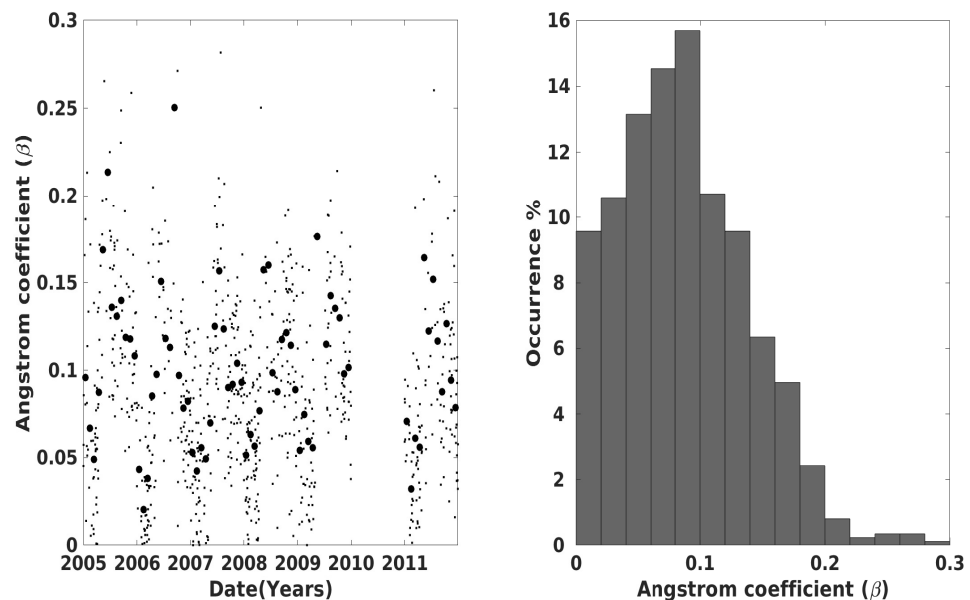


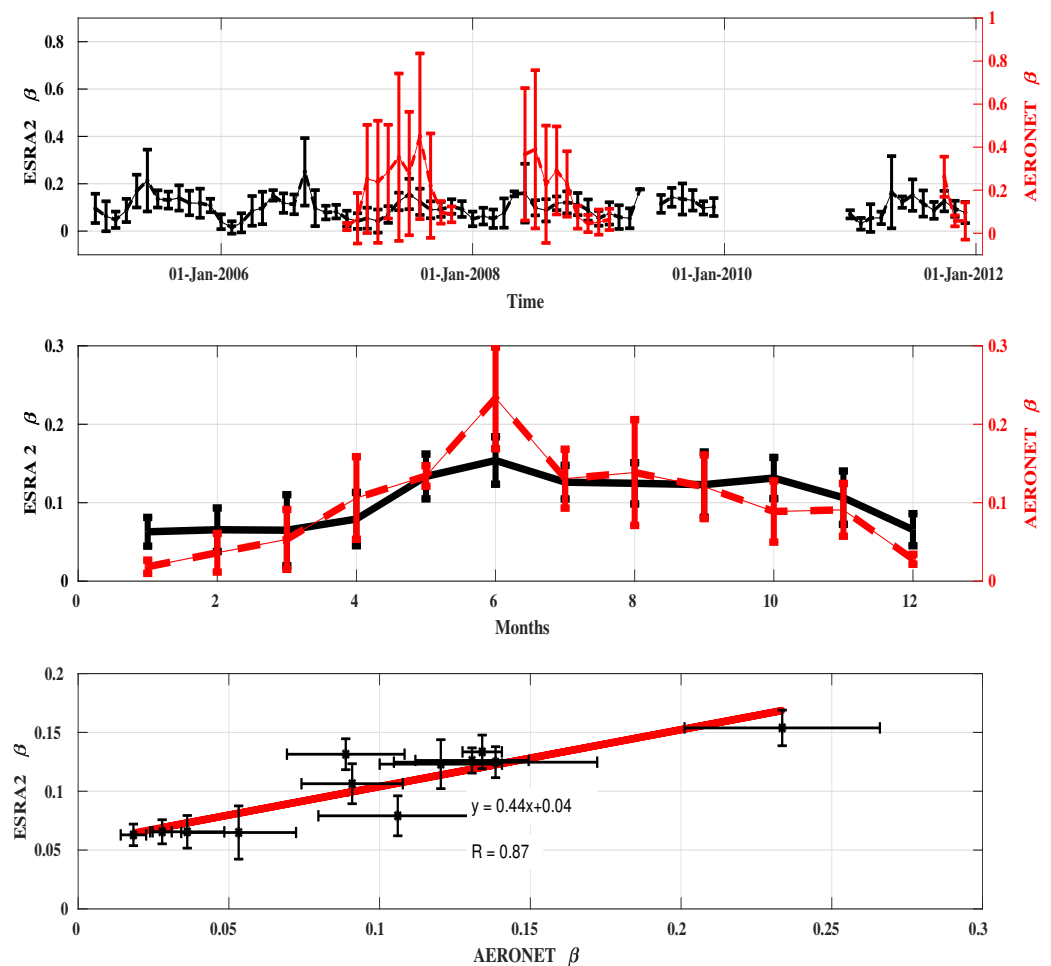
**Figure 7.** Left plot: daily variations of the Angström coefficient at Tamanrasset between 2005 and 2011. Right plot: Histogram of Angström coefficient values.

Daily and monthly variations of the Angström coefficient obtained from solar radiation measurements recorded at Tamanrasset are shown in Figure 8 (black curves). The monthly average values are given in Table 2. There are no values of the Angström coefficient in June 2009 due to the lack of clear days during this month. The red curves correspond to the Angström coefficient obtained from AERONET. In spite of the temporal discontinuities, we note that the monthly curves obtained with the ESRA model and AERONET are similar even if the values are higher for the latter. They have the same trend over the year. Indeed, the linear regression performed on  $\beta$  obtained with the ESRA model and AERONET have  $R$  value of 0.87 (see bottom plot in Figure 8). They have also their maximum values in June (middle plot in Figure 8). We can explain it by winds of the south sectors (Sirocco) during the summer season that characterize the Sahara of North Africa. This kind of winds brings particles of dust and sand with them, which increases the Angström coefficient [1,19,20,32,41].

The ESRA model shows a secondary  $\beta$  maximum during September–October months unlike AERONET. Differences in  $\beta$  obtained from AERONET are probably due to the low number of measurements at Tamanrasset between 2005 and 2011. Seasonal variations of the Angström coefficient can be explained by high temperatures in June in Tamanrasset (around 30 °C) combined with low values of humidity (around 10%) (top plot in Figure 9) and also the presence of dust storms during this month. We note that there is a temporal extremum of  $\beta$  (middle plot in Figure 8) while there is an extremum in both humidity and temperature at the same time (bottom plot in Figure 9). These seasonal variations are most likely related to the African monsoon [1,20,32,41,42].

**Table 2.** Monthly average values of the Angström coefficient.

Months	2005	2006	2007	2008	2009	2011
January	0.10 ± 0.06	0.09 ± 0.06	0.09 ± 0.06	0.07 ± 0.06	0.09 ± 0.06	0.09 ± 0.06
February	0.06 ± 0.04	0.08 ± 0.07	0.05 ± 0.04	0.06 ± 0.03	0.07 ± 0.06	0.06 ± 0.06
March	0.05 ± 0.03	0.05 ± 0.03	0.06 ± 0.04	0.14 ± 0.08	0.05 ± 0.04	0.06 ± 0.03
April	0.09 ± 0.05	0.09 ± 0.05	0.16 ± 0.05	0.13 ± 0.04	0.06 ± 0.04	0.08 ± 0.05
May	0.17 ± 0.07	0.17 ± 0.06	0.18 ± 0.09	0.15 ± 0.04	0.12 ± 0.01	0.16 ± 0.06
June	0.21 ± 0.13	0.21 ± 0.12	0.13 ± 0.04	0.12 ± 0.04	-	0.23 ± 0.10
July	0.14 ± 0.04	0.14 ± 0.03	0.15 ± 0.05	0.14 ± 0.05	0.17 ± 0.09	0.14 ± 0.03
August	0.13 ± 0.04	0.13 ± 0.04	0.12 ± 0.04	0.12 ± 0.05	0.15 ± 0.04	0.11 ± 0.03
September	0.14 ± 0.05	0.13 ± 0.04	0.11 ± 0.06	0.11 ± 0.06	0.12 ± 0.03	0.14 ± 0.04
October	0.12 ± 0.05	0.14 ± 0.04	0.09 ± 0.04	0.09 ± 0.04	0.14 ± 0.04	0.16 ± 0.08
November	0.12 ± 0.06	0.13 ± 0.05	0.02 ± 0.03	0.02 ± 0.02	0.14 ± 0.05	0.11 ± 0.04
December	0.11 ± 0.03	0.11 ± 0.05	0.03 ± 0.05	0.03 ± 0.03	0.12 ± 0.06	0.11 ± 0.05

**Figure 8.** Time variations (top), monthly average over 2005–2011 (middle), and linear regression (bottom) between the Angström coefficient obtained from ESRA2 model (black) and AERONET (red).

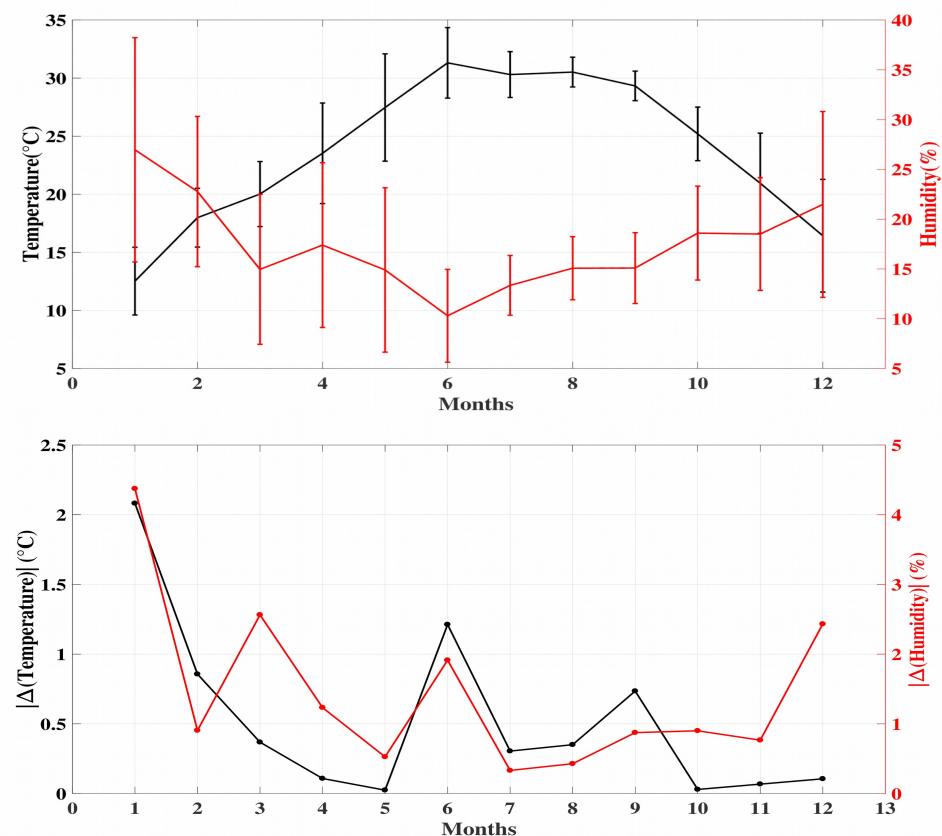


**Figure 9.** Top plot: Monthly average between 2005 and 2011 of the temperature (black line) and humidity (red line) recorded at the ground level at Tamanrasset. Bottom plot: The Laplacian of the monthly average temperature (black line) and humidity (red line) showing their local extrema.

Finally, we compared the Angström coefficient obtained with ESRA 2 model with the frequency of occurrence of aerosols over Tamanrasset observed from space. The DARDAR (raDAR/liDAR) products are used for this study [43–45]. The DARDAR product is a synergetic product that combines joint observations from the Cloud Profiling Radar (CPR) on board CloudSat and Cloud-Aerosol Lidar with Orthogonal Polarization on board CALIPSO, both located in the A-Train constellation of satellites [46,47]. DARDAR products take advantage of this combination to identify the cloud phase, precipitation, and aerosol within the column sampled by the two instruments. Using the mask in the DARDAR product, we derive an aerosol frequency of occurrence parameter, defined as the ratio of the number of aerosol occurrences in a domain of interest over the number of observations in that domain. A valid aerosol occurrence is an occurrence of at least three adjacent vertical pixels (to avoid artifacts) flagged with the “aerosol” category in the mask. Doing this for each month and each year, we built yearly averages and a four-year average of monthly time series of the frequency of occurrence of aerosol over a rectangular region of 1 degree by 1 degree located over the Tamanrasset. The period 2007–2010 is considered for the analysis of DARDAR products. The left plot in Figure 10 plots the time variation of the monthly average of the Angström coefficient  $\beta$  obtained using the ESRA 2 model together with the frequency of occurrence of aerosol over Tamanrasset, while the right plot shows the equivalent monthly average between 2007 and 2009. The analysis period 2007–2009 is considered since it is the common part of data. Interestingly, both curves have very similar shapes. This is confirmed by plotting  $\beta$  versus the frequency of occurrence of aerosol for which a linear variation is observed. Indeed, the approximation of the values by a straight line gives  $R = 0.70$  (Figure 11).

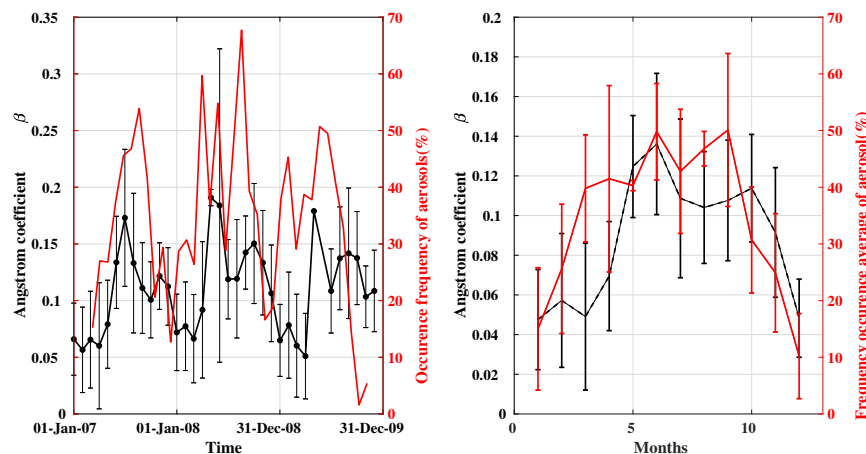


**Figure 10.** (Left): Time variations of the monthly average of  $\beta$  obtained from ESRA2 model (black) and frequency of occurrence of aerosols observed from space (red). (Right): Monthly average over 2007–2009 of  $\beta$  (black) and of the frequency of occurrence of aerosols (red).

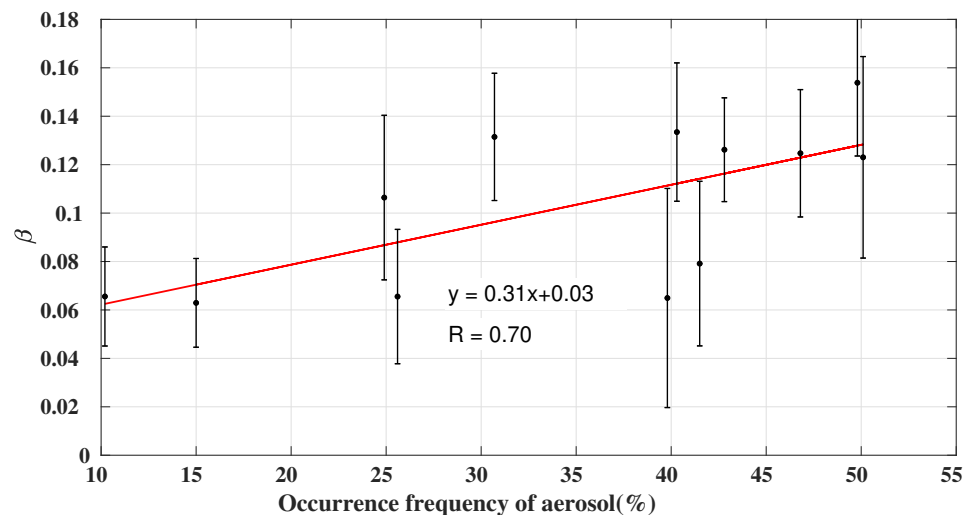


**Figure 11.** Correlation of the monthly average over the period from 2007 to 2009 of the Angström coefficient obtained from ESRA2, and the frequency of occurrence of aerosol over Tamanrasset observed with A–Train satellites.

## 5. Conclusions

This paper deals with the turbidity investigated with both models and measurements of the global solar radiation reaching the Earth's surface. The Linke turbidity factor is taken to quantify the transparency of the atmosphere. The Linke turbidity factor is first estimated considering several models that depend on it and that provide a good fit to global solar radiation measurements. The Kasten, Gistel, ESRA1, ESRA2 and Capderou models were used with measurements performed during the period 2005–2011 at Tamanrasset, southern Algeria, near the Tropic of Cancer. The results showed that the monthly average of the Linke turbidity factor has the same trend regardless of the models used, albeit with some differences. They therefore also showed the need to find the most reliable model for estimating the Linke turbidity factor. Two atmospheric parameters, the aerosol optical depth and the total column-integrated water vapor, obtained from AERONET and MODIS, respectively, were used to conduct a comparative study between the Linke turbidity factor and the joint radiation transmittance of these parameters. The Gistel and ESRA models appeared to have a better agreement between the variations of the Linke turbidity factor with those of the aerosol and water vapor joint transmittance, compared to what was obtained with the Kasten and Capderou models. We also found that their results were

very similar and that they gave the monthly mean value with the highest Linke turbidity factor of the year (in June), which also corresponded to the highest joint transmittance of the two parameters. We conclude that the Gistel and ESRA2 models were the most appropriate models for estimating the Linke turbidity factor with an advantage for the ESRA2 model revealed by the correlation with the joint transmittance of aerosol and water vapor. The Angström coefficient was then deduced from the Linke turbidity obtained from the ESRA2 model over the period 2005–2011. The results showed that 9% of Angström coefficients are less than 0.02 at Tamanrasset, 76% are between 0.02 and 0.15, and 13% are greater than 0.15. These values are very similar to those obtained in a previous work for Ghardaïa, located about 1100 km north of Tamanrasset [19]. The monthly average of the Angström coefficient obtained with ESRA2 also showed the same trend during the year with AERONET measurements and reached its maximum values in June. These seasonal variations are most likely related to the African monsoon.

Finally, we compared the Angström coefficient obtained with the ESRA 2 model to the aerosol frequency occurrence in Tamanrasset deduced from space observations of the A-Train satellites. A similar trend was observed for the Angström coefficient and the frequency of occurrence of aerosol. This was confirmed by plotting the Angström coefficient with respect to the frequency of occurrence of aerosol where a linear relationship was observed with  $R = 0.70$ .

**Author Contributions:** Methodology, M.Z. and A.I.; validation, M.Z., A.I., C.L. and J.D.; formal analysis, M.Z.; investigation, A.I.; resources, M.Z.; data curation, M.M. and S.B.B.; writing—original draft preparation, M.Z.; writing—review and editing, A.I., D.k., F.C. and D.D.; supervision, A.I.; funding acquisition, A.I. All authors have read and agreed to the published version of the manuscript.

**Funding:** This research received no external funding and The APC was funded by LATMOS

**Data Availability Statement:** The AERONET data used in this study is available from <http://aeronet.gsfc.nasa.gov>, accessed on 1 March 2021. The MODIS products used in this work are available from <https://earthdata.nasa.gov/>, accessed on 1 March 2021. For the meteorological and solar radiation data, the authors were unable to find a valid data repository for data used in this study. The data are available from Mr Mimouni Mohamed at Regional Meteorological Center (Direction météo Régional Sud, Office National de la Météorologie, ONM, Algeria).

**Acknowledgments:** The authors thank URAER and LATMOS (CNRS) for their support, which made this publication possible, as well as ONM of Tamanrasset for providing the data used in this study. DGK acknowledges support for this work by the project “PANhellenic infrastructure for Atmospheric Composition and climatE change” (MIS 5021516), which is implemented under the Action “Reinforcement of the Research and Innovation Infrastructure”, funded by the Operational Programme “Competitiveness, Entrepreneurship and Innovation” (NSRF 2014–2020) and co-financed by Greece and the European Union (European Regional Development Fund).

**Conflicts of Interest:** The authors declare no conflicts of interest.

## References

1. Trabelsi, A.; Masmoudi, M. An investigation of atmospheric turbidity over Kerkennah Island in Tunisia. *Atmos. Res.* **2011**, *22*, 101. [CrossRef]
2. Malik, A. A modified method of estimating Angström’s turbidity coefficient of solar radiation models. *Renew. Energy* **2000**, *21*, 537. [CrossRef]
3. Kaskaoutis, D.; Kambezidis, H.; Adamopoulos, A.; Kassomenos, P. Comparison between experimental data and modeling estimates of aerosol optical depth over Athens, Greece. *J. Atmos. Sol. Terr. Phys.* **2006**, *68*, 1167–1178. [CrossRef]
4. Kosmopoulos, P.; Kazadzis, S.; El-Askary, H.; Taylor, M.; Gkikas, A.; Proestakis, E.; Kontoes, C.; El-Khayat, M. Earth-Observation-Based Estimation and Forecasting of Particulate Matter Impact on Solar Energy in Egypt. *Remote Sens.* **2018**, *10*. [CrossRef]
5. Kambezidis, H.; Adamopoulos, A.; Zevgolis, D. Spectral aerosol transmittance in the ultraviolet and visible spectrum in Athens, Greece. *Pure Appl. Geophys.* **2005**, *162*, 625–647. [CrossRef]
6. Kaskaoutis, D.; Kambezidis, H.; Jacovides, C.; Steven, M. Modification of solar radiation components under different atmospheric conditions in the greater Athens area, Greece. *J. Atmos. Sol. Terr. Phys.* **2006**, *68*, 1043–1052. [CrossRef]
7. Kaskaoutis, D.; Kambezidis, H. Investigation on the wavelength dependence of the aerosol optical depth in the Athens area. *Q. J. R. Meteorol. Soc.* **2006**, *132*, 2217–2235. [CrossRef]

8. Kaskaoutis, D.; Kambezidis, H. The diffuse-to-global land diffuse-to-direct-beam spectral irradiance ratios as turbidity indexes in an urban environment. *J. Atmos. Sol. Terr. Phys.* **2009**, *71*, 246–256. [[CrossRef](#)]
9. Gueymard, C. Clear-sky irradiance predictions for solar resource mapping and large-scale applications: Improved validation methodology and detailed performance analysis of 18 broadband radiative models. *Sol. Energy* **2012**, *86*, 2145–2169. [[CrossRef](#)]
10. Antonanzas-Torres, F.; Urraca, R.; Polo, J.; Perpiñán-Lamigueiro, O.; Escobar, R. Clear sky solar irradiance models: A review of seventy models. *Renew. Sustain. Energy Rev.* **2019**, *107*, 374–387. [[CrossRef](#)]
11. Badescu, V.; Gueymard, C.; Cheval, S.; Oprea, C.; Baciu, M.; Dumitrescu, A.; Iacobescu, F.; Milos, I.; Rada, C. Computing global and diffuse solar hourly irradiation on clear sky: Review and testing of 54 models. *Renew. Sustain. Energy Rev.* **2012**, *16*, 1636–1656. [[CrossRef](#)]
12. Kambezidis, H.; Psiloglou, B.; Karagiannis, D.; Kaskaoutis, U.D.D. Recent improvements of the Meteorological Radiation Model for solar irradiance estimates under all-sky conditions. *Renew Energy* **2016**, *93*, 142–158. [[CrossRef](#)]
13. Kambezidis, H.; Psiloglou, B.; Karagiannis, D.; Dumka, U.; Kaskaoutis, D. Meteorological Radiation Model (MRM v6.1): Improvements in diffuse radiation estimates and a new approach for implementation of cloud products. *Renew. Sustain. Energy Rev.* **2017**, *74*, 616–637. [[CrossRef](#)]
14. Gueymard, C. *SMARTS2, A Simple Model of the Atmospheric Radiative Transfer of Sunshine: Algorithms and Performance Assessment*; Rep. FSEC–PF–270–95; Florida Solar Energy Center: Cocoa, FL, USA, 1995.
15. Linke, F. Transmissions-Koeffizient und Trübungsfaktor. *Beitr. Phys. Atmos.* **1922**, *10*, 91–103.
16. Angström, A. Techniques of determining the turbidity of the atmosphere. *Tellus* **1961**, *13*, 214. [[CrossRef](#)]
17. Ineichen, P.; Perez, R. A New Air Mass Independent Formulation For The Linke Turbidity Coefficient. *Sol. Energy* **2002**, *73*, 151–157. [[CrossRef](#)]
18. Cucumo, M.; Marinelli, V.; Oliveti, G. Data bank Experimental data of the Linke Turbidity factor and estimates of the Ångström turbidity coefficient for two Italian localities. *Renew. Energy* **1999**, *17*, 397–410. [[CrossRef](#)]
19. Djafer, D.; Irbah, A. Estimation of atmospheric turbidity over Ghardaïa city. *Atmos. Res.* **2013**, *128*, 76–84. 2013.03.009. [[CrossRef](#)]
20. Marif, Y.; Bechki, D.; Zerrouki, M.; Belhadj, M.; Bouguettaia, H.; Benmoussa, H. Estimation of atmospheric turbidity over Adrar city in Algeria. *J. King Saud Univ. Sci.* **2019**, *31*, 143–149. [[CrossRef](#)]
21. Chabane, F.; Moumami, N.; Brima, A. A New Approach to Estimate the Distribution of Solar Radiation Using Linke Turbidity Factor and Tilt Angle. *Trans. Mech. Eng.* **2021**, *45*, 523–534. [[CrossRef](#)]
22. Saad, M.; Trabelsi, A.; Masmoudi, M.; Alfaro, S.C. Spatial and temporal variability of the atmospheric turbidity in Tunisia. *J. Atmos. Sol. Terr. Phys.* **2016**, *149*, 93–99. [[CrossRef](#)]
23. Kambezidis, H.D.; Psiloglou, B.E. Climatology of the Linke and Unsworth—Monteith Turbidity Parameters for Greece: Introduction to the Notion of a Typical Atmospheric Turbidity Year. *Appl. Sci.* **2020**, *10*, 4043. [[CrossRef](#)]
24. Zakey, A.S.; Abdelwahab, M.M.; Makar, P.A. Atmospheric turbidity over Egypt. *Environment* **2004**, *38*, 1579–1591. [[CrossRef](#)]
25. Behar, O.; Sbarbaro, D.; Marzo, A.; Moran, L. A simplified methodology to estimate solar irradiance and atmospheric turbidity from ambient temperature and relative humidity. *Renew. Sustain. Energy Rev.* **2019**, *116*, 109310. [[CrossRef](#)]
26. Flores, J.L.; Karam, H.A.; Marques Filho, E.P.; Pereira Filho, A.J. Estimation of atmospheric turbidity and surface radiative parameters using broadband clear sky solar irradiance models in Rio de Janeiro-Brazil. *Theor. Appl. Climatol.* **2016**, *123*, 593–617. [[CrossRef](#)]
27. Meziani, F.; Boulifa, M.; Ameer, Z. Determination of the global solar irradiation by MSG-SEVIRI images processing in Algeria. *Energy Procedia* **2013**, *36*, 525–534. [[CrossRef](#)]
28. Mefti, A.; Adane, A.; Bouroubi, M. A Satellite approach based on cloud cover classification: Estimation of hourly global solar radiation from meteosat images. *Energy Convers. Manag.* **2008**, *49*, 652–659. [[CrossRef](#)]
29. Davies, J.; McKay, D. Evaluation of Selected Models for Estimating Solar Radiation on Horizontal Surfaces. *Sol. Energy* **1989**, *43*, 153–168. [[CrossRef](#)]
30. Rigollier, C.; Bauer, O.; Wald, L. On the clear sky model of the ESRA—European Solar Radiation Atlas— with respect to the heliosat method. *Sol. Energy* **2000**, *68*, 22–48. [[CrossRef](#)]
31. Capdrou, M. *Atlas Solaire de l'Algérie, Modèles Théoriques et Expérimentaux*; Office des Publications Universitaires: Algiers, Algeria, 1987; Volume 1.
32. Marif, Y.; Chiba, Y.; Belhadj, M.; Zerrouki, M.; Benhammou, M. Clear Sky Irradiation Assessment Using A Modified Algerian Solar Atlas Model in Adrar City. *Energy Rep.* **2018**, *4*, 84–90. [[CrossRef](#)]
33. Yaiche, M.; Bekkouche, A.B.S.; Malek, A.; Benouaz, T. Revised Solar Maps of Algeria Based on Sunshine Duration. *Energy Convers. Manag.* **2014**, *82*, 114–123. [[CrossRef](#)]
34. Brichambaut, P.; Vauge, C. *Le Gisement Solaire: évaluation de la ressource énergétique*. Lavoisier: Paris, France, 1982.
35. Zaiani, M.; Djafer, D. Atmospheric Turbidity Study Using Ground and Orbit Data. *Int. J. Latest Res. Sci. Technol.* **2014**, *3*, 12–18.
36. Zaiani, M.; Djafer, D.; Chouireb, F. New Approach to Establish a Clear Sky Global Solar Irradiance Model. *Int. J. Renew. Energy Res.* **2017**, *7*, 1454–1462.
37. Zaiani, M.; Djafer, D.; Chouireb, F.; Irbah, A.; Hamidia, M. New Method for Clear Day Selection Based on Normalized Least Mean Square Algorithm. *Theor. Appl. Climatol.* **2019**, 1–8. [[CrossRef](#)]
38. Iqbal, M. *An Introduction to Solar Radiation*; Academic Press: Toronto, ON, Canada, 1983.

39. Louche, A.; Maurel, M.; Simonnot, G.; Peri, G.; Iqbal, M. Determination of Ångström's turbidity coefficient from direct total solar irradiance measurements. *Sol. Energy* **1987**, *38*, 89–96. [[CrossRef](#)]
40. Lopez, G.; Battles, F. Estimate of the atmospheric turbidity from three broad-band solar radiation algorithms, a comparative study. *Ann. Geophys* **2004**, *22*, 2657–2668. [[CrossRef](#)]
41. Djelloul, D.; Abdanour, I.; Philippe, K.; Mohamed, Z.; Mustapha, M. Investigation of Atmospheric Turbidity at Ghardaïa (Algeria) Using Both Ground Solar Irradiance Measurements and Space Data. *Atmos. Clim. Sci.* **2019**, *9*, 114–134. [[CrossRef](#)]
42. Cuesta, J.; Edouart, D.; Mimouni, M.; Flamant, P.; Loth, C.; Gibert, F.; Marnas, F.; Bouklila, A.; Kharef, M.; Ouchène, B.; et al. Multiplatform observations of the seasonal evolution of the Saharan atmospheric boundary layer in Tamanrasset, Algeria, in the framework of the African Monsoon Multidisciplinary Analysis field campaign conducted in 2006. *J. Geophys. Res.* **2008**, *113*. [[CrossRef](#)]
43. Delanoë, J.; Hogan, R. Combined CloudSat-CALIPSO-MODIS retrievals of the properties of ice clouds. *J. Geophys. Res.* **2010**, *115*. [[CrossRef](#)]
44. Ceccaldi, M.; Delanoë, J.; Hogan, R.; Pounder, N.; Protat, A.; Pelon, J. From CloudSat-CALIPSO to EarthCare: Evolution of the DARDAR cloud classification and its comparison to airborne radar-lidar observations. *J. Geophys. Res.* **2013**, *118*, 7962–7981. [[CrossRef](#)]
45. Cazenave, Q.; Ceccaldi, M.; Delanoë, J.; Pelon, J.; Groß, S.; Heymsfield, A. Evolution of DARDAR-CLOUD ice cloud retrievals: New parameters and impacts on the retrieved microphysical properties. *Atmos. Meas. Tech.* **2019**, *12*, 2819–2835. [[CrossRef](#)]
46. Stephens, G.; Vane, D.; Boain, R.; Mace, G.; Sassen, K.; Wang, Z.; Illingworth, A.; O'Connor, E.; Rossow, W.; Durden, S.; et al. The CloudSat Mission and the A-Train. *Bull. Am. Meteorol. Soc.* **2002**, *83*, 1771–1790. [[CrossRef](#)]
47. Winker, D.; Pelon, J.; Coakley, J.; Ackerman, S.; Charlson, R.; Colarco, P.; Flamant, P.; Fu, Q.; Hoff, R.; Kit-taka, C.; et al. The CALIPSO Mission: A global 3D view of aerosols and clouds. *Bull. Am. Meteorol. Soc.* **2010**, *91*, 1211–1229. [[CrossRef](#)]